

Friction Stir Spot Welding of Al–Cu with Different Zn Foils

Hua Liu¹ · Lin Ma¹ · Peng Gong¹ · Jihong Dong^{2,3} · Yumei Yue¹

Received: 21 November 2021 / Accepted: 6 October 2022 / Published online: 8 November 2022
© The Indian Institute of Metals - IIM 2022

Abstract In order to improve the quality of friction stir spot welding joint of Al–Cu dissimilar metals, the pure Zn foils with different thicknesses were selected as the interlayer to perform the experiments. The thickness of Zn foil affected the morphology of the lap interface and the thickness of the intermetallic compound layer. The structure and composition of IMCs layer of Zn-added joint were similar when the thickness of Zn foil varied from 0.02 to 0.1 mm. The IMCs layer at the lap interface of the Zn-added joint was composed of $Al_xCu_yZn_z$, Al_2Cu , and $\alpha Al + Al_2Cu$ three sub-layers structure. The thickness of the IMCs layer increased with the increase in Zn thickness, and the joint obtained the smallest IMCs layer of 79 μm with the addition of 0.02 mm Zn foil. The joint with 0.02 mm Zn foil obtained the maximum tensile shear load of 6.84 kN, which was 0.52 kN bigger than that of the joint without Zn foil. The fracture mode of the joints with 0.02 and 0.05 mm Zn foils was the quasi-cleavage characterized by cleavage surface, granular fracture surface and large tearing ridge, while the joint with 0.1 mm Zn and the joint without Zn foil belonged to the cleavage fracture.

Hua Liu and Lin Ma contributed equally to this work.

✉ Peng Gong
Gongpeng2020@163.com

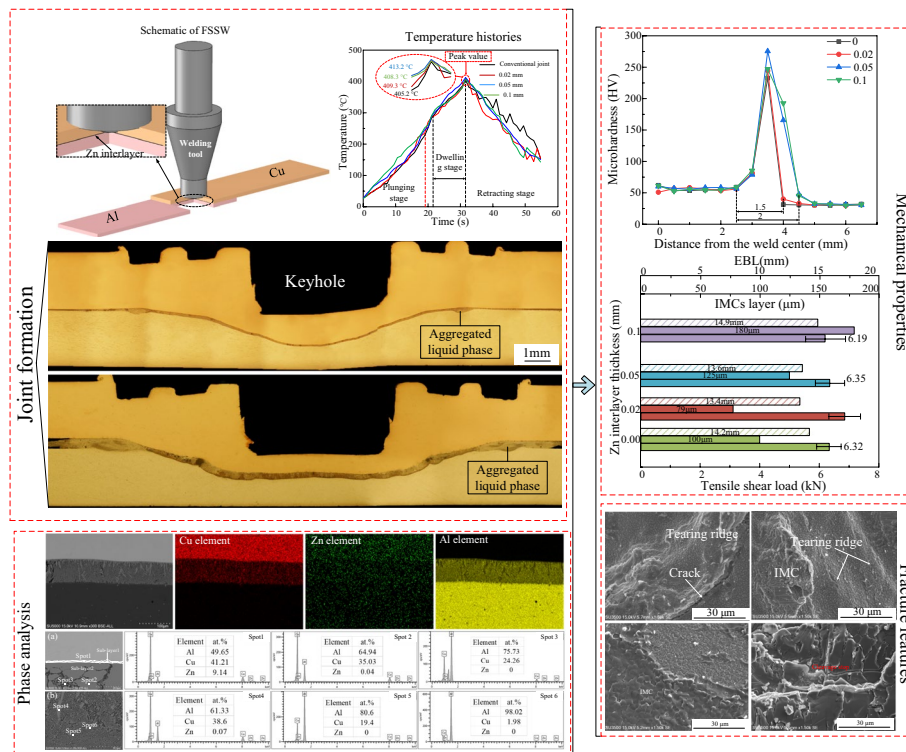
✉ Jihong Dong
dongjihong2021@163.com

¹ College of Aerospace Engineering, Shenyang Aerospace University, Shenyang 110136, People's Republic of China

² Beijing Institute of Petrochemical Technology, Beijing 102617, People's Republic of China

³ Beijing Academy of Safety Engineering and Technology, Beijing 102617, People's Republic of China

Graphical abstract



Keywords Al–Cu dissimilar metals joint · Friction stir spot welding · Zn foil · Mechanical properties · Interface microstructure

1 Introduction

Friction stir spot welding (FSSW) has the advantages of low welding temperature, strong plastic deformation and high joint performance, which is promising in the joining of aluminum and copper (Al–Cu) dissimilar metals [1, 2]. A high-quality Al–Cu joint can be obtained by FSSW [3], which provides broad application prospect in batteries, generators, substations, transformers and heat exchange equipment. However, the critical process parameters, such as the probe morphology, rotational velocity (RV), plunging depth (PD), plunging velocity (PV), and dwelling time (DT), control the joining process and influence the joint strength during the FSSW process [4–6]. Therefore, the process parameter's optimization of Al–Cu FSSW is utilized to improve the joining and promote the strength of dissimilar Al–Cu joint. The high-quality joint usually owns a continuous and uniform intermetallic compounds (IMCs) layer at the Al–Cu interface [7–9]. However, it is difficult to regulate the IMCs of the joint by only relying on the optimization of the parameters, so the improvement of joint performance is limited [10–12]. The auxiliary energy field and the assisted process are more appropriate for regulating the IMCs and improving mechanical properties of dissimilar Al–Cu joint.

The ultrasonic vibration and the addition of interlayer are mostly used in the welding for regulating the IMCs. Notably, the local abundant IMCs at the Al–Cu interface are the trigger for the crack, which has an adverse impact on the joint quality [10]. Zuo et al. [13] reported that the ultrasonic vibration could regulate the interfacial microstructure and break the IMCs particles. However, the unsuitable ultrasonic vibration can easily cause cracks at the lap interface, thereby weakening the joint quality. By comparison, the addition of interlayer is another feasible process. As reported [14–16], the Nickel (Ni), Titanium (Ti), and Zinc (Zn) foils as the interlayer were used to weld the dissimilar Al–Cu joint. Sahu et al. [15] reported that the joint tensile properties assisted by Ti and Zn foils were more superior due to the controlled flow of IMCs by diffused Ti foil and the thin, continuous, and uniform IMCs formation in the case of Zn foil. The melting point of Zn is lower than that of Al and Cu metals, and the thermal expansion coefficient of Zn is between Al and Cu metals [16]. It is believed that the molten Zn foil can act as an alloying element in the weld area, which is conducive to the release of residual stress and the improvement of the joint performance [17]. However, there are few related research works about the Al–Cu FSSW with the addition of Zn foil.

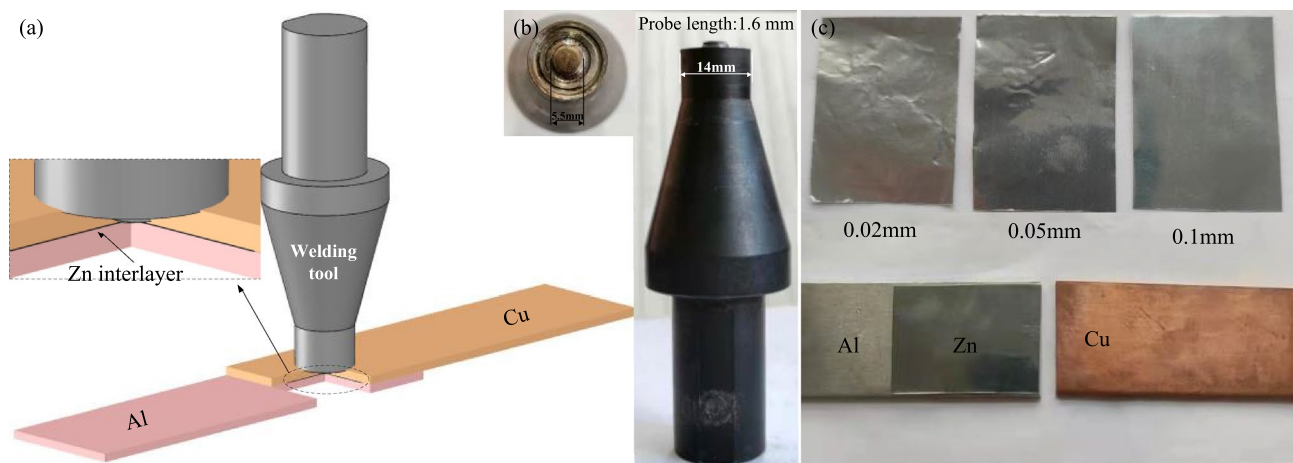


Fig. 1 Process of FSSW with Zn foil **a** schematic, **b** welding tool and **c** Zn foils used in experiments

In this study, the dissimilar Al–Cu joint was welded by the FSSW assisted by Zn foils with different thicknesses through pure diffusion bonding, which was mainly used to obtain sufficient joint strength. Therefore, the Cu/Al lap configuration (Cu sheet is on the top of Al sheet) not the conventional Al/Cu lap configuration (Al sheet is on the top of Cu sheet) was used. The aim of this research is a better understanding of the effect of the thickness of Zn foils on mechanical and metallurgical properties in the Al–Cu FSSW process.

2 Materials and Methods

The 1060 aluminum alloy and T2 pure copper sheets with the dimensions of 105 mm × 30 mm × 2 mm were employed as base materials (BMs). Figure 1a shows the schematic of FSSW. The Cu sheet was on the top of Al sheet, and the length of overlap area was 35 mm. The welding tool consisted of a taper pin with thread and a concave shoulder with concentric-circles groove. The diameters of tool shoulder, pin root and top were maintained to be 14 mm, 5.5 mm and 5.0 mm. The pin length of 1.6 mm was chosen, and the actual structure of the tool is shown in Fig. 1b. The pure Zn foils of a purity of 99.99% with the dimension of 30 mm × 35 mm were displayed at the center of the overlap area, and the thicknesses of them were 0.02, 0.05, and 0.1 mm, as shown in Fig. 1c. The welding process was conducted at the tool rotational velocity of 1500 rpm, the plunging rate of 5 mm/min, the dwell time of 10 s and tool shoulder plunge depth of 0.2 mm.

The cross section metallographic specimens were etched with the corrosive solution of 5 g FeCl_3 + 3 ml HCl + 10 ml $\text{C}_2\text{H}_5\text{OH}$ + 40 ml H_2O for 15 s for observing the microstructures of Cu BM. The IMCs at the lap interface were etched

with 2.5% HF solution for 10 s for better viewing by an optical microscope (OM). A scanning electron microscope (SEM) equipped with energy-dispersive spectroscopy (EDS) was used for phase analysis. Vickers microhardness distribution was measured along the lines on the cross section which were 1.5 and 3 mm above the bottom surface of the aluminum sheet under the test load of 100 g for 15 s. The detailed dimension of tensile shear specimen is displayed in Fig. 2. The tensile shear tests were performed at the loading rate of 2 mm/min by a universal mechanical tester. At the same time, the fracture morphology of Cu sheet was observed by the SEM. The temperature histories were recorded by K type thermocouples fixed at the lap interface, and the measuring point was 10 mm away from the center of the welding spot, as shown in Fig. 2.

3 Results and Discussion

3.1 Temperature Histories

Because the pin does not penetrate into the Cu sheet, the metallurgical bonding at the Al–Cu lap interface has the dominant effect on the joint quality. During the FSSW process of dissimilar Al–Cu joint, the elevated temperature is the precondition for plastic flow of materials and the atom diffusion, the nucleation and growth of IMCs at the lap interface [18]. Therefore, the temperature histories of Zn-added and conventional joints are shown in Fig. 3. Actually, the temperature histories of Zn-added and conventional joints have the identical regularity, and the addition of the Zn foil has no obvious effect on the variation in temperature. The peak temperatures of the measuring points are 409.3 °C, 413.2 °C, 408.0 °C and 405.2 °C, which is closed to the melting point of pure Zn of 419.7 °C. Due to the severe

Fig. 2 Detailed dimensions of tensile shear specimen and the schematic of temperature measuring point

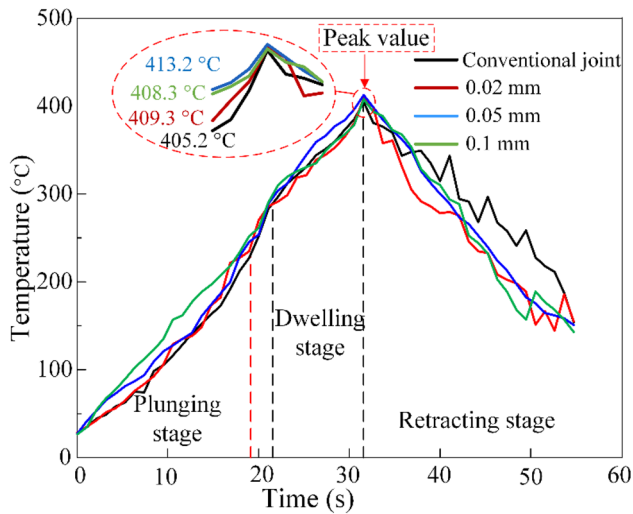
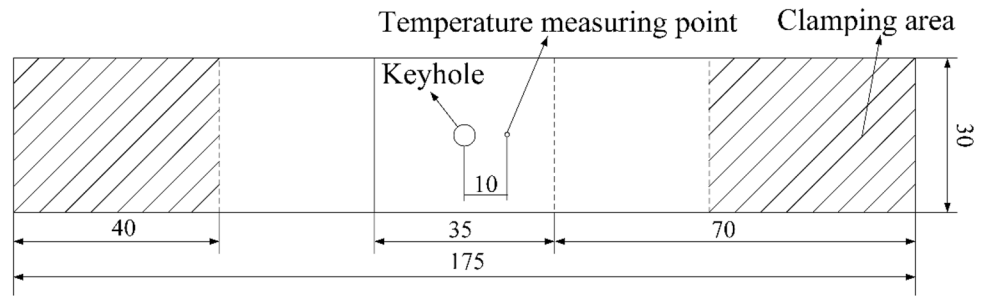


Fig. 3 Temperature histories of Zn-added and conventional joints

friction and stirring between the welding tool and the Cu metals, the temperature rises rapidly as the plunging depth increases. Under the plunging stage of tool pin, the temperature rises rapidly due to the severe friction and stirring between the tool pin and the Cu metals. Under the plunging stage of tool shoulder, the friction region continuously increases and the temperature also shows an obvious rise. However, the softening degree of Cu metals increases with the rising of temperature, and this softened material cause the decrease in the heat production rate. During the dwelling stage, the friction region is constant but the heat production rate decreases. Therefore, the friction heat still accumulates continuously but the rise rate of temperature is slower at this stage.

3.2 Joint Formations

The cross section of the upper part of Al–Cu joint with the 0.02 mm thickness Zn foil is shown in Fig. 4a. The cross section is divided into keyhole, shoulder stirring zone (SSZ), pin stirring zone (PSZ), thermo-mechanically affected zone

(TMAZ), heat affected zone (HAZ) and BM. The typical microstructures of different zones marked in Fig. 4a are displayed in Figs. 4b–g. Owing to the high temperature and the complex material flow, the SSZ (Fig. 4b) and the PSZ are composed of the fine equiaxed grains but are inhomogeneous. The grain in PSZ2 (Fig. 4d) is bigger than that in PSZ1 (Fig. 4c) because the material flow in PSZ1 is more violent than that in PSZ2. The BM (Fig. 4e) is characterized by grains with many annealing twins. Compared to the BM, the HAZ (Fig. 4f) exhibits the coarsened grain. The microstructure of the TMAZ is shown in Fig. 4g, and the grains do not exhibit the elongated distributed along the flow lines but the equiaxed-recrystallized grains.

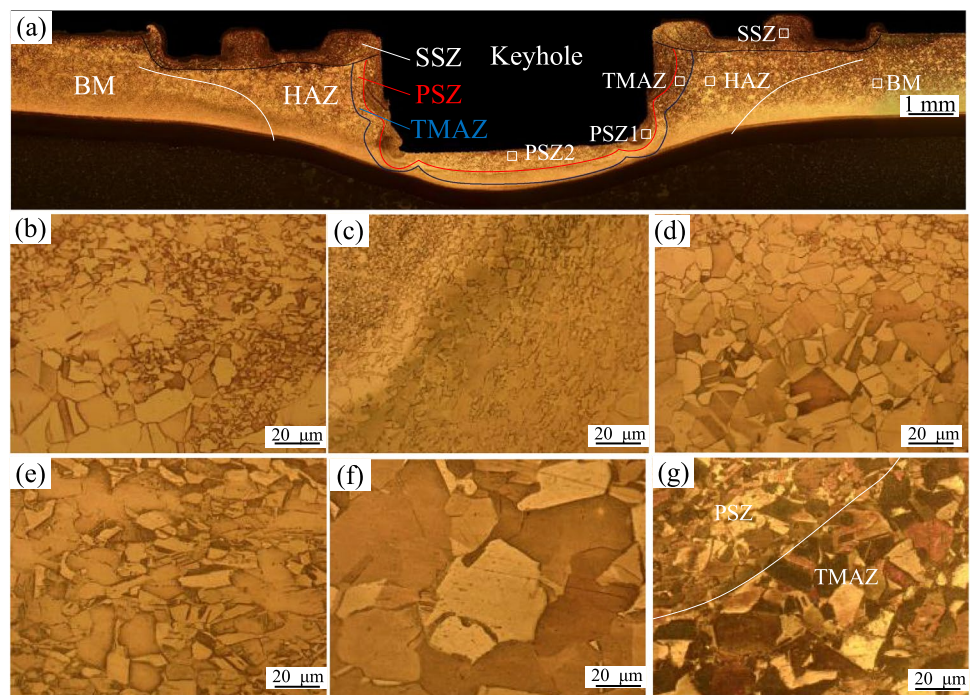
The lap interfaces of Zn-added and conventional joints are displayed in Fig. 5, and they are curved downward under the effect of welding tool. The molten liquid phase can be considered as a buffer, which can weaken the extrusion effect from the plasticized Cu metal and absorb the forging force from the welding tool. Thence, the lap interface under the keyhole of Zn-added joint with 0.1 mm Zn foil is almost the horizontal because large amounts of liquid phase are formed.

The aggregated liquid phase like drops is observed at the lap interface, and the peripheral regions of the drop-like liquid phase do not achieve effective bonding (Fig. 4a). Therefore, the drops-like liquid phase is the edge of the effective bonding region, and the distance between two symmetrical drop-like liquid phases is regarded as the effective bonding length (EBL) of the welding spot. Xue et al. [19] pointed that the larger bonding area is brought about a high joint strength. The joint with the addition of 0.02 mm Zn foil has the smallest EBL of 13.4 mm and the joint with 0.1 mm Zn foil has the biggest EBL of 14.9 mm. However, the hard and brittle IMCs layer at the lap interface is the key factor determining joint strength. The final effects of the EBL and thickness of IMCs layer on the tensile properties are explained in the following section.

3.3 Interfacial Microstructures and Phase Analysis

In order to reveal the evolution of the interfacial microstructure, the lap interface is divided into the area A (under

Fig. 4 Cross section with 0.02 mm Zn foil **a** Cu BM and the typical microstructures of **b** SSZ, **c** PSZ1, **d** PSZ2, **e** BM, **f** HAZ, **g** TMAZ



the probe) and area B (under the shoulder), as shown in Fig. 6. The microstructures of IMCs layer in area A and area B under different Zn foils are displayed in Fig. 7. The IMCs layer thickness in area A of Zn-added joint is 79 μm (Fig. 7a), 125 μm (Fig. 7b), 180 μm (Fig. 7c), and the thickness in area B is 124 μm (Fig. 7e), 154 μm (Fig. 7f), 285 μm (Fig. 7g). The thicknesses of IMCs layers in areas A and B of conventional joint are 100 μm (Fig. 7d) and 145 μm

(Fig. 7h). All the IMCs layers are divided into three layers including the sub-layer1, sub-layer2 and sub-layer3. The sub-layer1 is characterized by the continuous thin IMC, and the sub-layer2 is characterized by continuous but unevenly distributed IMC. The phase composition and structure of sub-layer3 are complicated, and they are mainly composed of the dendrite eutectic and lamellar eutectic. The distribution of these eutectics in sub-layer 3 at different Zn foils is

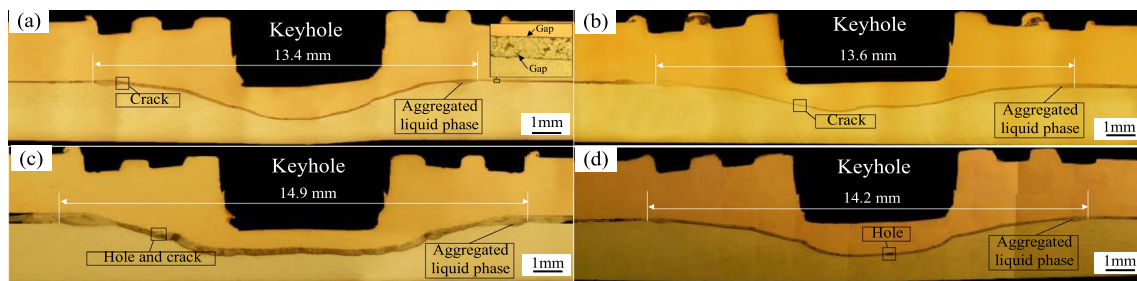
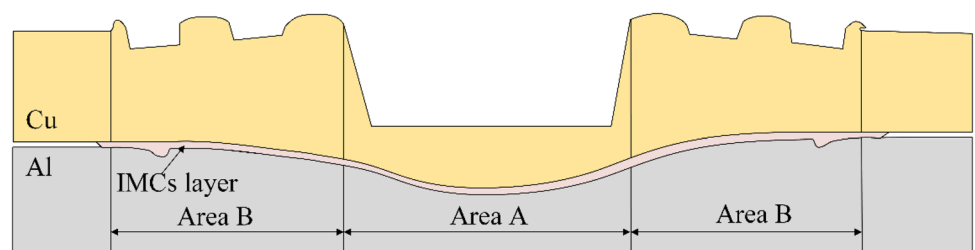


Fig. 5 Cross sections of joints under different thicknesses of Zn foils: **a** 0.02 mm, **b** 0.05 mm, **c** 0.1 mm and **d** conventional joint

Fig. 6 Schematic of lap interface division



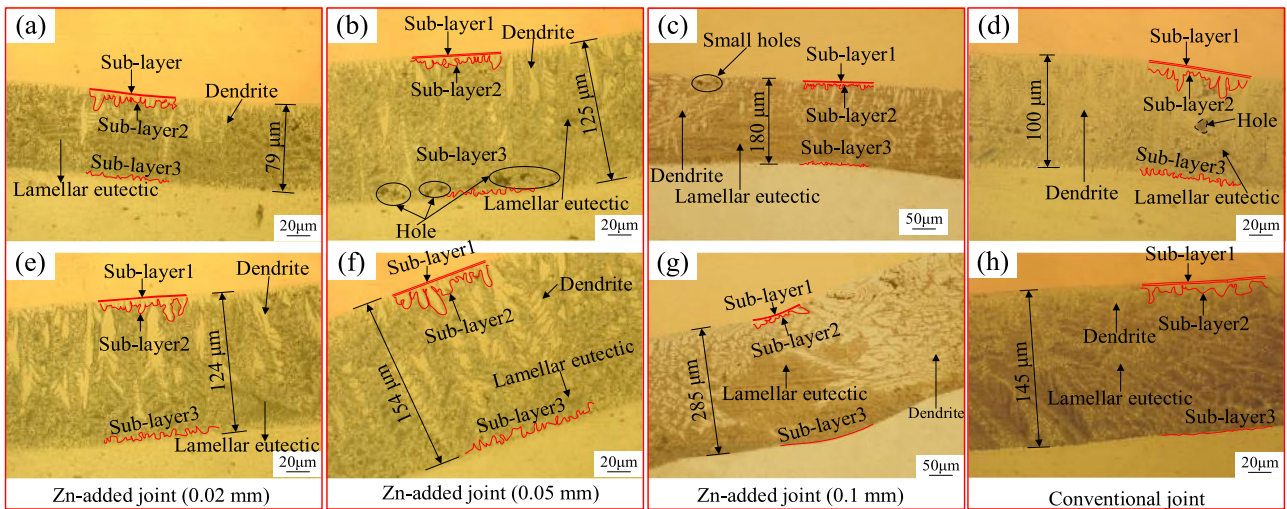
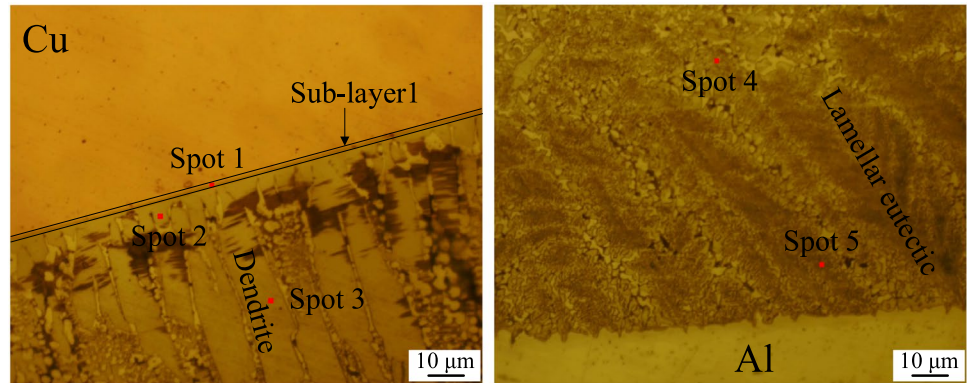


Fig. 7 Interface microstructures under different Zn foils: **a–d** located in area A, **e–h** located in area B

Fig. 8 Schematic of EDS scanning spots in conventional joint



different. In order to understand the composition of IMCs, the EDS was used for element analysis.

The schematic of EDS scanning spots in the conventional joint is shown in Fig. 8 and the EDS results are shown in Table 1. The molten Al metal as well as the inter-diffusion and reaction between Al and Cu elements result in this IMCs layer. The sub-layer1 is composed of the AlCu phase and the sub-layer2 consists of the Al₂Cu phase. The dendrite and lamellar eutectic in sub-layer 3 is the grown Al₂Cu phase and αAl + Al₂Cu eutectic, respectively. These results are also reported by Anna et al. [12] and Zuo et al. [13].

The area scanning results of Zn-added joints with 0.02 and 0.1 mm Zn foils are shown in Fig. 9. The IMCs layer distributed in the lap interface consists of three elements: Cu, Zn and Al. The Cu substrate contains dominant Cu as well as a small amount of Zn, and the Al substrate contains dominant Al as well as a small amount of Zn. However, the content of Zn element in Cu substrate is more than that in Al substrate. The Al element almost does not diffuse into the Cu

substrate as well as the Al substrate hardly has any Cu element. Actually, the composition and structure of the IMCs layers at different Zn foils are similar, because the contents of the Zn element have no big difference (Fig. 9).

In order to identify the content elements of different sub-layers and structures, the spot scanning is adopted to determine the elemental component. The spot scanning results of the joint with 0.02 mm and 0.1 mm Zn foil are shown in

Table 1 The EDS results of conventional joint

Locations	Element (at. %)		Composition
	Al	Cu	
Spot 1	44.02	55.92	AlCu
Spot 2	65.01	34.99	Al ₂ Cu
Spot 3	66.19	33.81	Al ₂ Cu
Spot 4	79.12	20.88	(Al) + Al ₂ Cu
Spot 5	81.16	18.84	(Al) + Al ₂ Cu

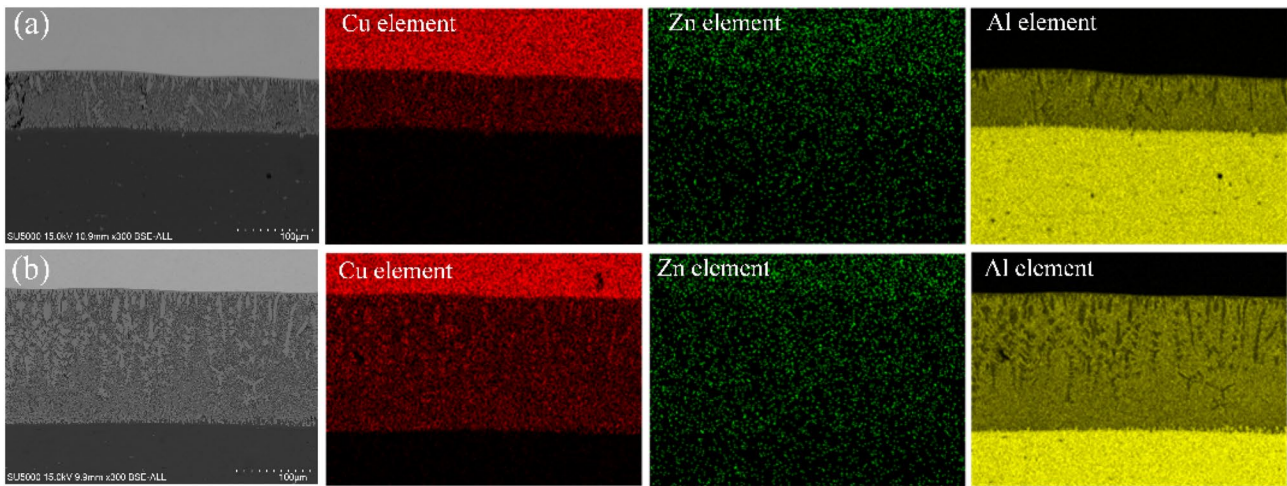


Fig. 9 Area scanning results the joints with **a** 0.02 Zn foil and **b** 0.1 mm Zn foil

Fig. 10. According to the results of scanning spots 1 and 2, the sub-layer1 consists of the $Al_xCu_yZn_z$ eutectic owing to the addition of Zn foil. However, the sub-layer2 is still the Al_2Cu phase, the dendrite is still the dispersed Al_2Cu phase and the lamellar eutectic is still composed of the $Al + Al_2Cu$ phase. The formation mechanism of the IMCs layer during welding process with Zn foil is similar to the study of Chen et al. [20]. The Zn metal melts firstly and the Zn elements spread to Cu and Al substrates. At the same time, the Cu and Al elements start dissolving into Zn liquid. Then, with the increase in the heat, the temperature continues to rise and the inter-diffusion of these three elements intensifies, and the Al metal starts to melt. The elaborate chemical reactions occur in the diffusion layer, finally the IMCs layer shown in Fig. 7 is formed. In fact, the stable phase of Al_2Cu can be formed directly after the eutectic temperature of $Al-Cu$

system (548 °C). In addition, due to the low content of Zn element, $CuZn_5$ phase which is founded in the study of Chen et al. [20] cannot be formed in this joint.

Actually, the volume of liquid Zn has the dominated influence on the thickness of the IMCs layer et al. $Al-Cu$ interface. Firstly, Zn element can inhibit the reaction between Al and Cu elements and then reduces the thickness of $Al-Cu$ IMCs layer. Moreover, the liquid Zn determines the thickness of eutectic layer produced during Zn solidification. The smaller the volume of liquid Zn, the smaller the thickness of eutectic layer. Thence, when the 0.02 mm, 0.05 mm and 0.1 mm Zn foils are adopted, the minimum IMCs layer is formed with the addition of 0.02 mm thick Zn foil.

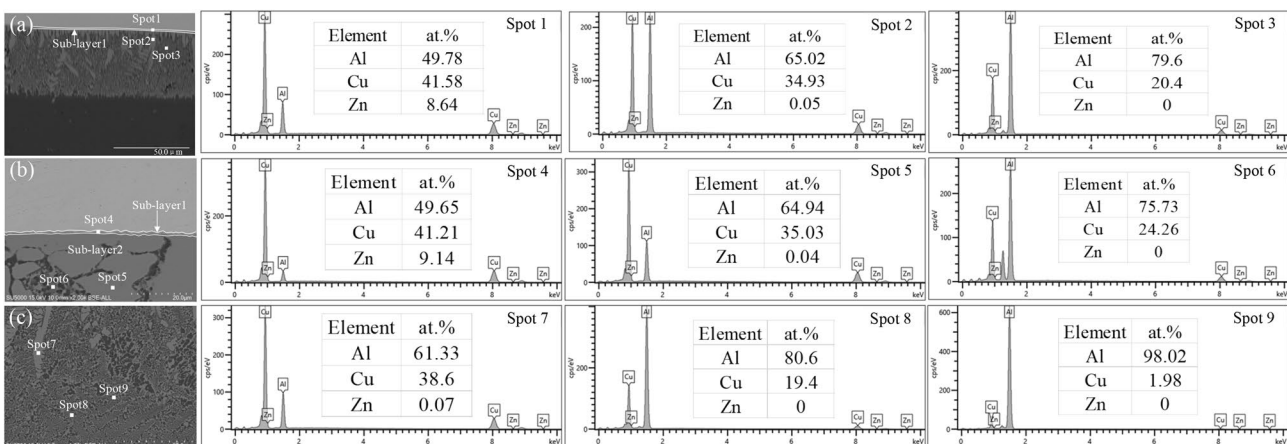


Fig. 10 The EDS results of joint with **a** 0.02 mm Zn foil and **b** 0.1 mm Zn foil

3.4 Microhardness Distributions

Figure 11 displays the schematic of microhardness-measured points and microhardness distributions of the joint with different Zn foils. Owing to the microstructure symmetry about the centerline of the welding spot, only the microhardness at the right side has been measured, and the measured lines are 3 mm (line A) and 1.5 mm (line B) away from the bottom surface of the Al sheet, as shown in Fig. 11a. Figure 11b shows the diamond indentation after measurement. Line A is located in the middle part of Cu sheet, and the correlation between the microhardness (Fig. 11c) and the grain size (Fig. 4) is evident. The microhardness in PAZ has the maximum value which corresponds to the refined grain (Figs. 4b, c), and the reason for the minimum microhardness in HAZ is the grown grain (Fig. 4f). In addition, the grain in TMAZ (Fig. 4g) is larger than that in BM (Fig. 4e). Consequently, the microhardness in TMAZ is lower than that in BM. On the other side, the annealing softening also plays a role in the low microhardness value in TMAZ and HAZ. The line B

starts from the centerline of the joint and passes through the IMCs layer. The microhardness in the line B distributes as the “A” shape and the IMCs layer has the biggest microhardness value. However, the measuring spots in the IMCs layer are different because of the different IMCs layer thicknesses, so the biggest microhardness value of 275.5 HV is obtained with the addition of 0.05 mm Zn foil.

3.5 Tensile Properties of the Joints

The tensile shear load (TSL) and the load–displacement curve of the Al–Cu lap joint with different Zn foils are displayed in Fig. 12. The TSL of conventional joint is 6.32 kN, and the TSLs of joints with 0.02, 0.05, 0.1 mm thick Zn foils are 6.84, 6.35 and 6.19 kN, respectively. The high TSL corresponds to the large displacement, as shown in Fig. 12b. Further, the maximum value of 6.84 kN is obtained with the addition of 0.02 mm Zn foil, while the TSL decreases to 6.19 kN after the 0.1 mm Zn foil is used. The principal reason for this regular is the thickness of IMCs layer at

Fig. 11 Microhardness-measured points **a** schematic and **b** diamond indentation; microhardness distributions along **c** line A and **d** line B

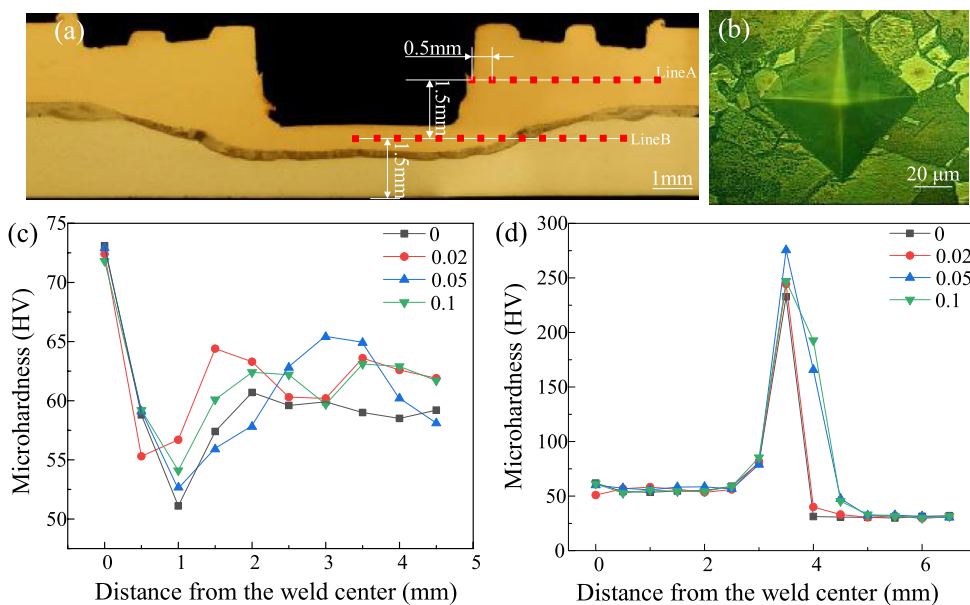
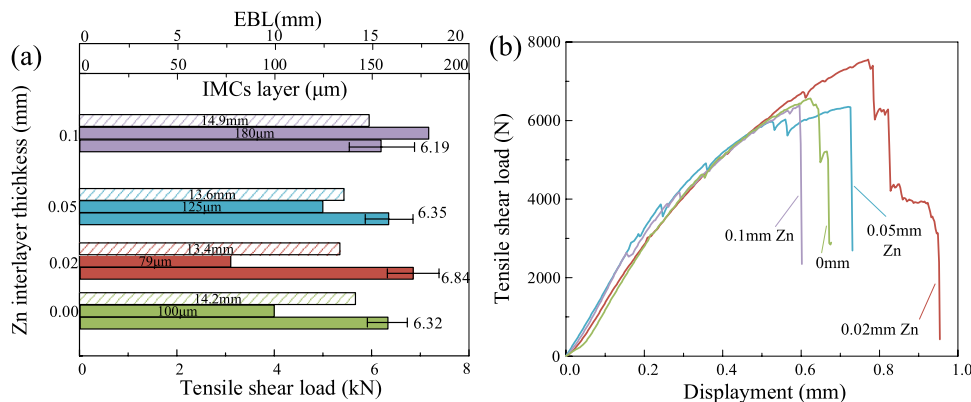


Fig. 12 Tensile properties under different thicknesses of Zn foils **a** average tensile shear load and **b** tensile shear load–displacement curves



the Al–Cu lap interface. The formation of a thin, continuous and uniform Al–Cu IMCs layer is conducive to form a good metallurgical bonding, but excessive (thick) IMCs are always detrimental to the joint performance. In fact, hard and brittle Al–Cu IMCs are the weak areas at the lap interface because they introduce high stress concentration and residual stress. The interface between the continuous Al_2Cu layer-BM, between Al_2Cu –AlCu, and between $Al_xCu_yZn_z$ and BM is often the crack source and crack propagation path when the joint is under load. The thickness of the IMCs layer in the Zn-added and conventional joints are more than $79\ \mu m$. Thence, the thickness of the IMCs is smaller, while the value of TSL is bigger, as shown in Fig. 12a. In addition, although the large EBL contributes to the high TSL, the effect of IMCs layer on TSL is dominant.

3.6 Fracture Features

The fracture surfaces of Al and Cu sheets at different thickness of Zn foils are shown in Fig. 13. From a macro-point of view, all the joints fracture at the Al–Cu lap interface. The lower surfaces of Cu sheet at different thickness of Zn foils are shown in Fig. 14. Because of the thick IMCs layer at the Al–Cu lap interface, the interface region makes the tensile specimen show the brittle fracture. The joint with 0.02 mm Zn foil shows the quasi-cleavage fracture surface, both cleavage surface and lager tearing ridge are observed (Fig. 14a and e). The fracture surface of the joint with 0.05 mm Zn foil under the keyhole also belongs to the quasi-cleavage fracture mode (Fig. 14b), while the surface under the shoulder changes to the cleavage fracture mode (Fig. 14g). As for the joint with 0.1 mm Zn foil, the too thick IMCs layer makes the granular fracture (Fig. 14c), and the cleavage step

Fig. 13 Fracture surfaces under different thicknesses of Zn foils **a** 0.02 mm, **b** 0.05 mm, **c** 0.1 mm and **d** conventional joint

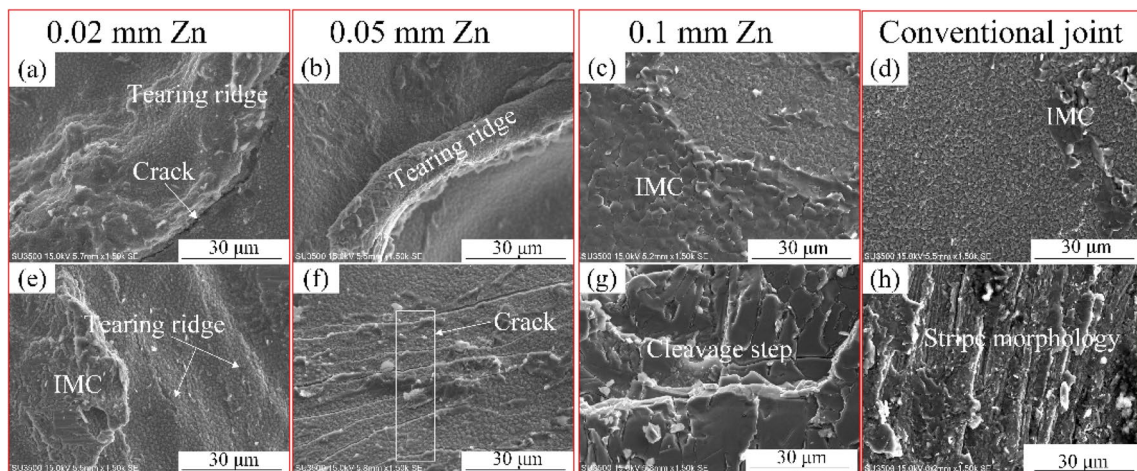
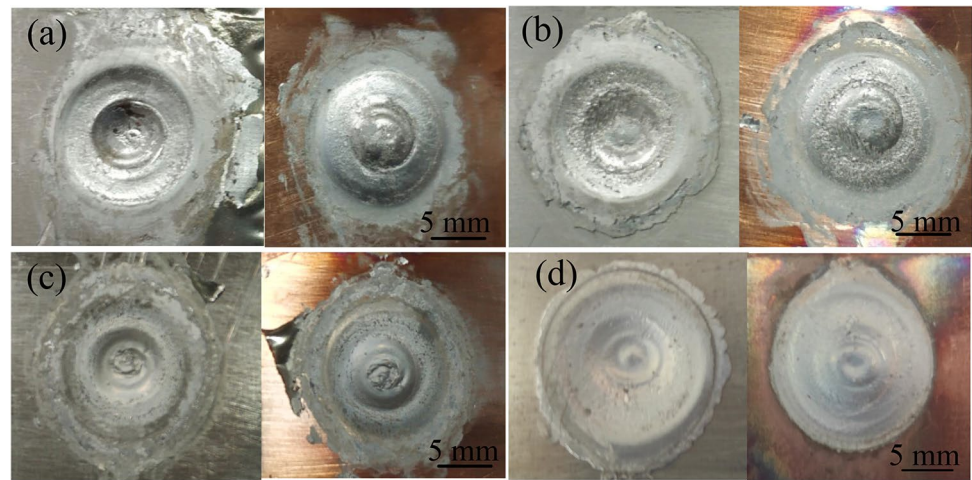


Fig. 14 Fracture surface morphologies of Cu sheet: **a–c** under the keyhole, and **e–g** under the shoulder of Zn-added joint; **d** under the keyhole and **h** under the shoulder of convention joint

(Fig. 14g) can be seen on fracture surfaces. In the case of conventional joint, the SEM analysis shows that the intergranular fracture (Fig. 14d) is the main character of the surface under the keyhole, while joint rupture changes to cleavage fracture with stripe morphology under the shoulder (Fig. 14h).

The hard and brittle IMCs in the lap interface lead to a brittle fracture mode dominated by granular fracture surface and cleavage surface. The addition of proper Zn foil makes the lager tearing ridge structure occur at the fracture surface and then improve the joint strength. However, too thick Zn foil also leads to a brittle fracture mode dominated by granular fracture surface and cleavage surface.

4 Conclusions

- (1) During the FSSW process, the Zn and Al metals both melted under the high temperature. The effective bonding length (EBL) of Al–Cu joint with 0.02 mm Zn foil was smallest of 13.4 mm, while the joint with 0.1 mm Zn foil had the biggest EBL of 14.9 mm.
- (2) A thick IMCs layer was formed at the Al–Cu lap interface. Compared with the conventional joint, the additional Zn foil changed the morphology, composition and thickness of IMCs layer. The joint with 0.02 mm Zn foil had the smallest IMCs layer of 79 μm , while the joint with 0.1 mm Zn foil had the biggest value of 180 μm .
- (3) For the Zn-added joints, the tensile shear load of the Al–Cu joint reached the maximum value of 6.84 kN when the 0.02 mm Zn foil was added. The joints all fractured at the Al–Cu lap interface, and the fracture mode of the high-quality joint was the quasi-cleavage fracture mode under the rational thickness of Zn foil.

Acknowledgements This project was funded by the National Natural Science Foundation of China (No. 51874201) and the Program for Liaoning Innovative Talents in University (LR2019049)

References

1. Meng X, Huang Y, Cao J, Shen J, dos Santos JF, *Prog Mater Sci* **115** (2021) 100706. <https://doi.org/https://doi.org/10.1016/j.pmatsci.2020.100706>
2. Li M, Zhang C, Wang D, Zhou L, Wellmann D, Tian Y, *Materials* **13** (2019) 156. <https://doi.org/https://doi.org/10.3390/ma13010156>

3. Heideman R, Johnson C, Kou S, *Sci Technol Weld Joining* **15** (2010) 597. <https://doi.org/https://doi.org/10.1016/j.compositesa.2017.12.005>
4. Huang Y, Meng X, Xie Y, Wan L, Lv Z, Jian Cao, Jicai Feng, *Compos Part A-Appl S* **105** (2018) 235. <https://doi.org/https://doi.org/10.1016/j.compositesa.2017.12.005>
5. D'Urso G, *J Manuf Process* **17** (2015) 108–119. <https://doi.org/https://doi.org/10.1016/j.jmapro.2014.08.004>
6. Lin YC, Liu JJ, Lin BY, *Adv Mater Res* **579** (2012) 109. <https://doi.org/https://doi.org/10.4028/www.scientific.net/AMR.579.109>
7. Li GH, Li Z, Zhou WL, Song XG, Huang YX, *J Mater Res Technol* **8** (2019) 2613. <https://doi.org/https://doi.org/10.1016/j.jmrt.2019.02.015>
8. Zhou L, Zhang R, Li G, Zhou W, Huang Y, Song X, *J Manuf Process* **36** (2018) 1. <https://doi.org/https://doi.org/10.1016/j.jmapro.2018.09.017>
9. Abbass M K, Hussein S K, Kudair A A, *Int J Eng Sci Res Technol* **4** (2015) 514. <https://www.researchgate.net/publication/291346102>
10. Manickam S, Rajendran C, Balasubramanian V, *Heliyon* **6** (2020) e04077. <https://doi.org/https://doi.org/10.1016/j.heliyon.2020.e04077>
11. Sun H, Zhou Q, Zhu J, and Peng Y, *J Mater Eng Perform* **26** (2017) 5715. <https://doi.org/https://doi.org/10.1007/s11665-017-3029-4>
12. Anna R, Franziska P, Tobias B, Pierre BJ, *Weld World* **63** (2019) 117. <https://doi.org/https://doi.org/10.1007/s40194-018-0620-8>
13. Zuo YY, Gong P, Ji SD, Li QH, Lv Z, *J Manuf Process* **62** (2021) 58. <https://doi.org/https://doi.org/10.1016/j.jmapro.2020.11.019>
14. Akbari M, Bahemmat P, Haghpanahi M, *Sci Technol Weld Joining* **18** (2013) 518. <https://doi.org/https://doi.org/10.1179/1362171813Y.0000000130>
15. Sahu PK, Pal S, Pal SK, *Metall Mater Trans A* **48** (2017) 3300. <https://doi.org/https://doi.org/10.1007/s11661-017-4093-y>
16. Huang G, Feng X, Shen Y, Zheng Q, Zhao P, *Mater Des* **99** (2016) 403. <https://doi.org/https://doi.org/10.1016/j.matdes.2016.03.094>
17. Kuang B, Shen Y, Chen W, Xin Y, Xu H, Gao J, Zhang J, *Mater Des* **68** (2015) 54. <https://doi.org/https://doi.org/10.1016/j.matdes.2014.12.008>
18. Boucherit A, Abdi S, Aissani M, Mehdi B, Badji R, *Int J Adv Manuf Technol* **111** (2020) 1553. <https://doi.org/https://doi.org/10.1007/s00170-020-06202-z>
19. Xue P, Xiao B, Wang D, Ma Z Y, *Sci Technol Weld Joining* **16** (2011) 657. <https://doi.org/https://doi.org/10.1179/1362171811y.0000000018>
20. Chen S, Wang D, Li R, Liu B, Wang J, *J Mater Eng Perform* **28** (2019) 5245. <https://doi.org/https://doi.org/10.1007/s11665-019-04244-3>

Publisher's Note Springer Nature remains neutral with regard to jurisdictional claims in published maps and institutional affiliations.

Springer Nature or its licensor (e.g. a society or other partner) holds exclusive rights to this article under a publishing agreement with the author(s) or other rightsholder(s); author self-archiving of the accepted manuscript version of this article is solely governed by the terms of such publishing agreement and applicable law.